Carbon 247 (2026) 121023

Contents lists available at ScienceDirect

Carbon

journal homepage: www.elsevier.com/locate/carbon

Quantifying the effects of geometric parameters on the bending stiffness of multilayer graphene platelet films

Penghao Qi [a], Xindong Chen [a,b], Hanxing Zhu [a,*], Yongtao Lyu [c,d], Qing Peng [e]

[a] School of Engineering, Cardiff University, Cardiff, CF24 3AA, UK
[b] Institute of Biomechanics and Medical Engineering, AML, Department of Engineering Mechanics, Tsinghua University, Beijing, 100084, China
[c] Department of Engineering Mechanics, Dalian University of Technology, No. 2 Linggong Road, 116024, Dalian, China
[d] State Key Laboratory of Structural Analysis for Industrial Equipment, Dalian University of Technology, No. 2 Linggong Road, 116024, Dalian, China
[e] School of Power and Mechanical Engineering, Wuhan University, Wuhan 430072, China

ARTICLE INFO

Keywords:
Multilayer graphene platelet films
Bending stiffness
Size effects
Defect effects
Deformation mechanisms
Finite element simulation

ABSTRACT

Multilayer graphene platelet films (MGPFs) are widely used in many different applications like flexible electronics and bendable devices, however, the bending stiffness of MGPFs could significantly affect the functions and reliability of such products. Although some 2D models have been developed to investigate the effects of geometric parameters and component material properties on the bending stiffness of graphene films, these 2D models can't correctly capture the actual 3D geometric characteristics of MGPFs and thus may not be able to accurately predict the bending stiffness of MGPFs. In this work, thousands of realistic multiscale 3D geometric models are constructed to perform finite element simulations and quantify the effects of geometric parameters and component material properties on the bending stiffness of MGPFs, the obtained results are normalized by those of the perfect large-sized graphene films and compared with those available in literature. The developed models and the obtained results apply not only to MGPFs, but also to other types of multilayer laminate composites such as MXene, graphene oxide films and nacre-like materials. The results provide guidelines for the optimal design of MGPFs and other laminate composites, enabling their potential in diverse applications.

1. Introduction

Two-dimensional (2D) nanosheets such as graphene, MXenes, and hexagonal boron nitride (h-BN) can be assembled into multilayer van der Waals materials that have attracted widespread attention due to their excellent flexibility and processability [1,2]. Among them, graphene stands out for its extraordinary mechanical strength, electrical and thermal conductivity, optical transparency, and flexibility. However, the fabrication of large-area, defect-free graphene remains a significant challenge. As a practical alternative, multilayer graphene platelet films (MGPFs) have emerged as promising candidates for flexible electronic applications, where their mechanical adaptability is particularly well-suited to the demands of next-generation wearable devices, sensors, and soft robotics. To fully harness their potential, a thorough understanding and optimization of their bending behaviour is essential, as flexural performance directly impacts the reliability and service life of such devices [3–5]. Inspired by natural materials like nacre [6], researchers have attempted to mimic hierarchical structures in multilayer graphene-based films to enhance their mechanical robustness. While significant progress has been made, much of the existing research concentrates on enhancing interlayer bonding [7,8], often neglecting the intricate nanoscale geometries that play a critical role in effective stress transfer between nanosheets. This oversight contributes to the persistent disparity between theoretical predictions and actual performance [9]. Moreover, flexible devices typically require simultaneous optimization of mechanical, thermal, and electrical properties, presenting a multidimensional design challenge [10–13].

Although both experimental studies and atomistic simulations have provided valuable insights into the behaviour of multilayer graphene and natural lamellar structures, there remains a lack of effective multiscale models that link the nanoscale architecture to the macroscale mechanical performance [14–19]. In particular, accurately characterizing and predicting the out-of-plane bending stiffness remains a critical challenge. Most theorical calculation research based on 2D models [19–21], such as tension-shear model, are widely used for their simplicity but fail to account for the complex three-dimensional (3D)

* Corresponding author.
E-mail address: Zhuh3@cardiff.ac.uk (H. Zhu).

https://doi.org/10.1016/j.carbon.2025.121023
Received 28 August 2025; Received in revised form 26 October 2025; Accepted 1 November 2025
Available online 1 November 2025

architectures and non-uniform deformation patterns inherent in the bio-inspired MGPFs. These 2D models inadequately capture the localized stress concentrations and the impact of geometric parameters like platelet overlap and in-plane arrangement. Conversely, while molecular dynamics (MD) simulations can capture the atomic-scale deformation and interfacial behaviour, they are computationally intensive, suitable for models containing less than 1 million atoms, and limited in scalability, making them unsuitable for modelling the macroscopic behaviour or informing the engineering-level designs [22]. Therefore, there is a pressing need to develop reliable multiscale computational models capable of capturing both the local and global mechanical responses of MGPFs.

This study, for the first time, uses realistic multiscale 3D random nacre-like structural models to systematically investigate the bending stiffness of MGPFs, in which the individual graphene platelets are modelled as thin stiff shells and the van der Waals interaction between the staggered graphene platelets is represented by a single layer of equivalent soft solid material. Thousands of finite element simulations are performed, and the effects of different geometric parameters on the bending stiffness of MGPFs are systematically examined and quantified. It is noted that it is not feasible to use atomistic simulation to obtain all the required data in this work because each structural model contains over a billion atoms. This multiscale approach enables accurate simulation of the macroscale mechanical behaviour of MGPFs based on their nanoscale design features. The insights gained provide a foundation for the rational design of high-performance MGPFs tailored for flexible electronics and other advanced applications.

2. Multiscale geometric model and finite element treatment

Finite element method (FEM) is employed to quantify the effects of different geometric parameters on the bending stiffness of multilayer graphene platelet films (MGPFs). This section briefly introduces the construction of multiscale geometric models for MGPFs, the detailed treatment of the finite element simulations, and the mechanical properties of the constituent materials in the FEM models.

2.1. Basic geometric model and finite element treatment

In our previous work [23], a 3D periodic nanoscale multilayer representative volume element (RVE) model was developed to quantify the effects of different geometric parameters on the five independent elastic properties of MGPFs. In this study, a higher-level 3D structural model composed of three identical basic nanoscales periodic multilayer RVEs is adopted to capture the nanoscale geometric characteristics of MGPFs, and to quantify the effects of the different geometric parameters on the bending stiffness of MGPFs.

In the basic 3D nanoscale periodic RVE model with M layers of graphene and an in-plane side length of L, each layer is composed of N complete random Voronoi graphene platelets with the minimum distance δ between the centers of any neighboring graphene platelets. If all the graphene platelets are identical hexagons, the distance between the centers of the neighboring graphene platelets will be $d_0 = \boldsymbol{2L}/\left(\sqrt{\boldsymbol{2\sqrt{3}N}}\right)$. Thus, the degree of regularity of the random graphene platelets in the basic nanoscale RVE model is defined as $\alpha = \delta/d_0$ [24], and α is the same for the random graphene platelets in each layer of the same basic REV model. If $\alpha = 1$, all the platelets are identical regular hexagons, while $\alpha = 0$ represents completely random irregular polygons with 3–11 sides [24]. In the basic nanoscale RVE model of MGPFs with random irregular graphene platelets, the mean size of the graphene platelets is determined as d_0, in addition, the neighboring random Voronoi graphene platelets in each layer are assumed to have the same uniform intralayer gap which is assumed to be 1 nm or larger so that the intralayer interaction force between the intralayer neighboring graphene platelets can be ignored [25]. The area fraction of the graphene platelets in the basic RVE model is defined as [23]:

$$\boldsymbol{F_A} = \sum_{i=1}^{N} \boldsymbol{A_i} \Big/ \boldsymbol{L^2} \tag{1}$$

where A_i are the areas of all the individual graphene platelets in the same layer, and L^2 is the in-plane area of the basic nanoscale RVE model. For a given value of F_A, the uniform gap between any two intralayer neighboring graphene platelets can be easily determined.

Another important geometric parameter of the 3D periodic basic nanoscale RVE model of MGPFs is the graphene platelet overlap ratio ρ, which is defined as [23]:

$$\boldsymbol{\rho} = \boldsymbol{A_{overlap}} \big/ \boldsymbol{L^2} \tag{2}$$

where $A_{overlap}$ is the total overlap area of the staggered graphene platelets in two neighboring layers of the basic nanoscale RVE model. Obviously, ρ is corelated to F_A, and it has been found [23] that there exists the relation $\rho \propto F_A^2$.

The commercial ABAQUS 2022 finite element software is used to perform the finite element analyses. Each of the individual graphene platelets is meshed into an equivalent single layer of S4R shell elements, and the interlayer van der Waals interaction force between the staggered graphene platelets is represented by a single layer of C3D8R solid elements. To ensure the same out-of-plane bending stiffness ($B_1 = 2.385 \times 10^{-19} Nm$) and in-plane stretching stiffness ($D = 340$ N/m) of monolayer graphene, the thickness of the shell elements is determined as 0.09029 nm, and the Young's modulus of the equivalent shell solid material is obtained as 3.7656 TPa. The equivalent solid layer for van der Waals interaction has a thickness of $t = 0.34$ nm and a Young's modulus of 10 GPa according to the relevant literature [23,26,27]. The Poisson's ratio is 0.178 for the equivalent shell material and 0.001 for the equivalent solid material of van der Waals interaction [23]. It is noted that the equivalent C3D8R solid elements for van der Waals interaction between the staggered graphene platelets have common/shared notes with the equivalent S4R shell elements of these staggered graphene platelets. In addition, the S4R shell elements have overlap in space with the C3D8R solid elements in the finite element model, however, this does not cause any issue in the computational simulation of the ABAQUS software.

2.2. Higher-level structural model

This work aims to quantify the effects of different nanoscale geometric parameters of the basic RVE model, such as mean graphene platelet size d_0, regularity degree of graphene platelets α, graphene area fraction F_A, the number of complete graphene platelets N in each layer, and the number of graphene layers M, on the bending stiffness of MGPFs. Thus, both realistic basic nanoscale RVE model and higher-level structural model, as well as suitable boundary conditions are critical in FEM simulations in order to obtain accurate and useful results. In the 3D multilayer periodic basic nanoscale RVE model, each layer is a 2D periodic square Voronoi model with the same combination of geometric parameters L, d_0, α, F_A and N. Ideally, pure bending boundary conditions should be applied to the basic nanoscale RVE model to obtain the effective bending stiffness of the MGPF, however, it is very difficult to accurately apply such boundary conditions to the 3D basic nanoscale RVE model in finite element simulations. If the single 3D basic nanoscale RVE model is modelled as a cantilever structure with all the nodes on the lefthand side surface fixed, either concentrated load or another type of boundary conditions applied to the nodes on the righthand side surface of the RVE model, as shown in Fig. 1a, would have a great impact on the accuracy of the obtained effective bending stiffness of the MGPF. To minimize the effects of the applied boundary conditions, the same periodic $L \times L$ basic nanoscale RVE model of MGPFs is repeated several times along the span direction to make up a higher-level $3L \times L$ structural model in this work, as illustrated in Fig. 1b. Based on a comparison

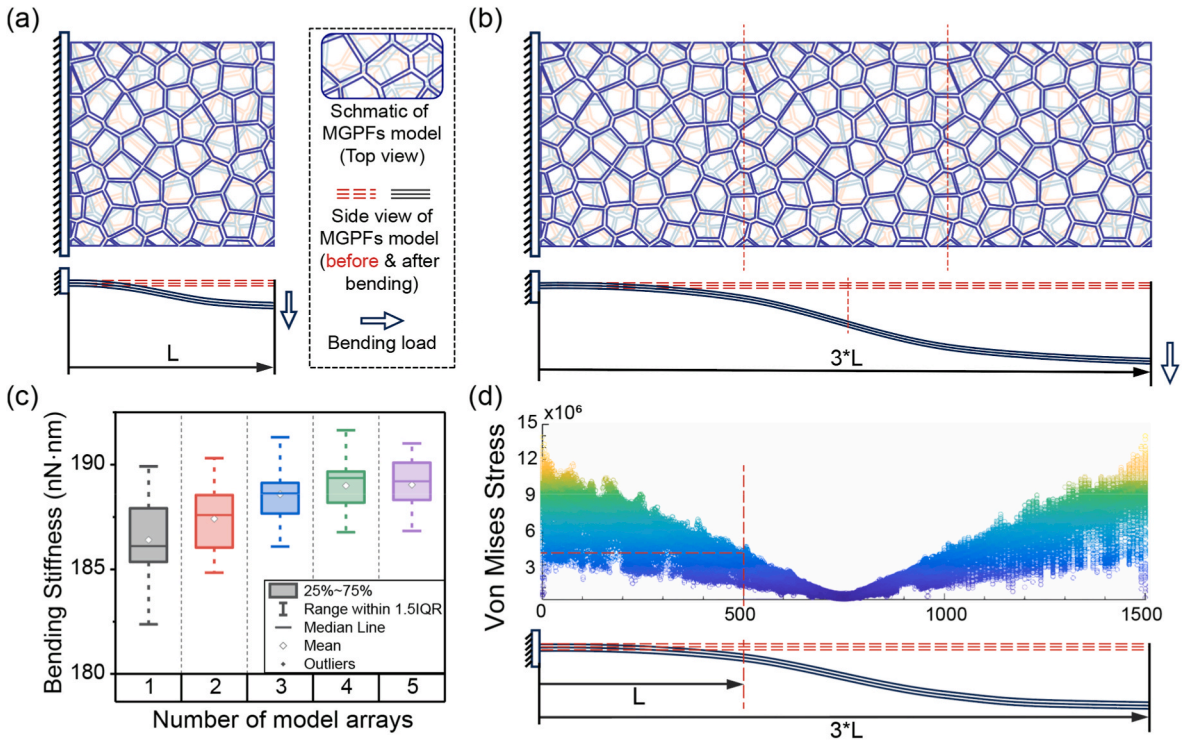

Fig. 1. Schematics of (a) the single basic nanoscale random periodic RVE model, and (b) the higher-level rectangular $3L \times L$ structural model with three repeated basic RVEs. (c) Effect of repetition times of the basic nanoscale periodic RVE model with $M = 4$, $d_0 = 106.5$ nm, $\alpha = 0.6$ and $N = 49$ on the obtained effective bending stiffness of MGPFs. (d) The magnitude of the bending stress in the whole lefthand side and righthand side basic RVEs is larger than 30 % of the maximum von Mises stress.

of the simulation results under different repetition counts of the same periodic basic nanoscale RVE model, it was found that when the repetition count is greater than or equal to 3, the simulation results of the higher-level structural model tend to converge as illustrated in Fig. 1c. Besides, based on the stress distribution in the higher-level rectangular $3L \times L$ structural model as shown in Fig. 1d, the magnitude of the bending stress in the whole lefthand side and righthand side basic nanoscale RVEs are larger than 30 % of the maximum von Mises stress in the whole structural model. Therefore, considering the computational efficiency and simulation accuracy, in all the simulations of this work, we choose to repeat 3 times of the same periodic basic nanoscale RVE for the higher-level rectangular $3L \times L$ structural model, as shown in Fig. 1b, in all the simulations of MGPFs in this work. All the degrees of freedom are fixed for the nodes on the lefthand side surface, while for all the nodes on the righthand side surface, all the other degrees of freedom are fixed except for a prescribed small vertical displacement Δ. Periodic boundary conditions are applied to all the corresponding nodes on the front and back surfaces, and all the nodes on the top and bottom surfaces are left unconstrained. Thus, according to the applied vertical displacement Δ, the reaction force F obtained from finite element simulation and the dimensions of the rectangular structural model (*i.e.* $3L \times L$), the bending stiffness of MGPFs can be obtained as $B_{Eff} = 2.25FL^3/\Delta$. Some relevant information is also provided in Fig. S1in the supporting Information.

2.3. Number of platelets in each layer

In this study, increasing the number N of the complete graphene platelets per layer in the basic nanoscale RVE model allows for a more accurate representation of the nanostructure of MGPFs and more precise prediction of the mechanical properties such as the bending stiffness. However, a larger number N also increases the computational cost and complexity, making large-scale simulations more time-consuming. Therefore, selecting an optimal number of complete graphene platelets N per layer is crucial to balance accuracy and computational efficiency in the analyses. In this regard, the bending stiffnesses of MGPFs with different numbers of complete graphene platelets N in each layer of the basic nanoscale RVE are simulated and their relationship is plotted in Fig. 2.

As can be seen in Fig. 2, the bending stiffness of the MGPF model is significantly influenced by the number of complete graphene platelets

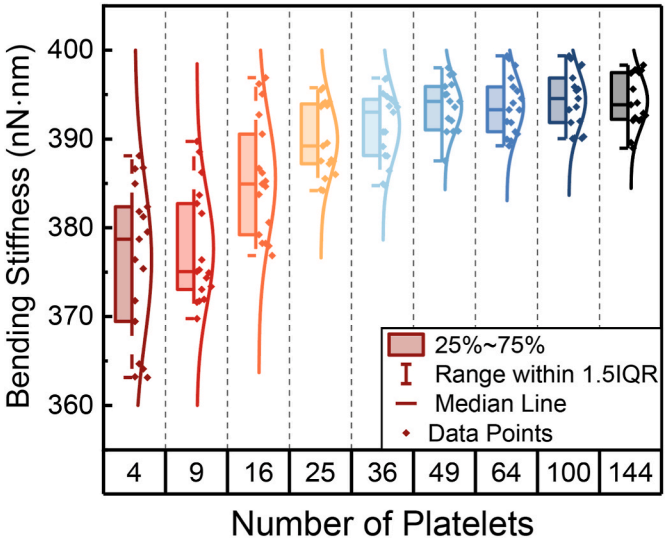

Fig. 2. Effects of the number of complete graphene platelets N in each layer of the basic nanoscale RVE model on the effective bending stiffness of MGPFs. The basic nanoscale RVE models have the same number of graphene layers $M = 5$, area fraction $F_A = 0.987$, degree of regularity $\alpha = 0.6$, and mean graphene platelet size $d_0 = 150$ nm.

per layer N of the basic nanoscale RVE when $N < 36$, leading to considerable fluctuations in both the average values and the stability of the results. Additionally, the limited number of complete graphene platelets fails to fully capture the geometric characteristics of the nacre-like MGPF, resulting in the calculated bending stiffness deviating from the overall value. Therefore, the number of complete graphene platelets is chosen as $N = 49$ for each graphene layer in all the basic nanoscale $L \times L$ RVE models of MGPFs to ensure a balance between high computational accuracy and manageable computational cost.

2.4. Mesh sensitivity analysis of numerical models

To obtain stable numerical results, a mesh sensitivity analysis was carried out for different mesh sizes as shown in Fig. 3. The basic nanoscale RVE model has a number of graphene layers $M = 5$, a mean size of graphene platelets $d_0 = 150$ nm, number of complete graphene platelets in each layer $N = 49$ and graphene platelet regularity degree $\alpha = 0.6$. The obtained bending stiffness of MGPFs is normalized by the bending stiffness of the perfect large-sized multilayer graphene films (B_M) given by Refs. [19,28]:

$$B_M = MB_1 + \frac{Dt^2}{12(1-\nu^2)}\left(M^3 - M\right) \tag{3}$$

Where M is the number of graphene layers; B_1 is the out-of-plane bending stiffness of perfect monolayer graphene and chosen as 2.385×10^{-19} Nm [16,19] in this work; $D = 340$ N/m [29], $\nu = 0.178$ [30] and $t = 0.34$ nm are the in-plane tensile stiffness and Poisson's ratio of monolayer graphene, and the interlayer space of neighboring graphene sheets, respectively. It is noted that we have performed finite element simulations to model the small curvature bending of large-sized perfect multilayer graphene films with different numbers of graphene layers M, the obtained bending stiffness results agree very well those given by Equation (3).

As can be seen in Fig. 3a and b, the computational results of the normalized bending stiffness of the MGPF model gradually converge as the mesh size decreases and the number of elements increases. However, Fig. 3b indicates clearly that the computational cost grows exponentially with the increase of the mesh density. Thus, a rational choice of mesh density is very important because the effects of different geometric parameters, such as larger graphene platelet diameter and larger number of graphene layers, will be investigated, and moreover, thousands of simulations will be performed to obtain all the required data in this work. It is noted that it is not feasible to use atomistic simulation to obtain all the required data in this work because each structural model contains over a billion atoms.

It should be noted that due to the complex model structure and deformations, the simulation results of the bending stiffness may be biased slightly higher than the actual values because of the mesh density. However, the trend and stability of the results are little affected by mesh size variations when the number of elements is sufficiently large. As demonstrated in Fig. 3a, the model data are relatively stable when the total number of the S4R shell elements in each graphene layer of the higher-level rectangular structural model ($3L \times L$) and the C3D8R solid elements in each equivalent solid layer for the van der Waals interaction between the staggered graphene platelets exceeds 96,000. The present study is more focused on the influence trends of different geometric parameters on the bending stiffness of the MGPF models. To compromise between the computational cost, the accuracy and reliability of the obtained data, this study adopts the mesh density as marked in Fig. 3a and b.

3. Results and discussion

3.1. Effects of the mean size of graphene platelets

During the assembly preparation of MGPFs, the mean size (or diameter) of graphene platelets can deviate significantly due to the differences in precursor materials and preparation processes. The different mean diameters will lead to a great difference in the overall structure and properties of the MGPFs. With this scenario, the bending stiffnesses of the MGPF models with different mean sizes of graphene platelets were calculated based on finite element method simulations. Fig. 4 plots the effective bending stiffnesses of MGPF models with two-to six-graphene layers as functions of the dimensionless mean size of graphene platelets (d_0/l_0), where $l_0 = \sqrt{Dt/(4G_{vdW})} = 2.404$ nm is the shear-lag characteristic length [31,32], D is the in-plane tensile stiffness (*i.e.,* 340 N/m) of the graphene platelets, t is the interlayer space between the staggered neighboring graphene platelets (*i.e.,* the thickness of the van der Waals interaction layer 0.34 nm), and G_{vdW} is the shear modulus (*i.e.,* 5 GPa) of the equivalent elastic solid material of the van der Waals interaction layer [23].

In Fig. 4, the effective bending stiffness B_{Eff} of the MGPFs increases sharply with the increasing dimensionless mean graphene platelet size when d_0/l_0 is small, gradually levels off when d_0/l_0 reaches a threshold value of 60, and approaches the values of the large-sized perfect multilayer graphene films when d_0/l_0 tends to infinity. It is noted that the results in Fig. 4 are approximately 2 % larger than the actual values owing to the effects of the mesh size/density. However, as the intralayer graphene platelet gap always weakens the in-plane tensile stiffness and the out-of-plane bending stiffness of the structural model, the bending stiffness of the MGPF with very large d_0/l_0 is still slightly (about 1 %) smaller than that of the large-sized perfect multilayer graphene film.

The relation between B_{Eff} and d_0/l_0 in Fig. 4 is very similar to that between the in-plane Young's modulus E_{11} and d_0/l_0 in Fig. 2 of literature [23].This is because when the structural model of MGPF is bent, the individual graphene platelets undergo in-plane tension or compression,

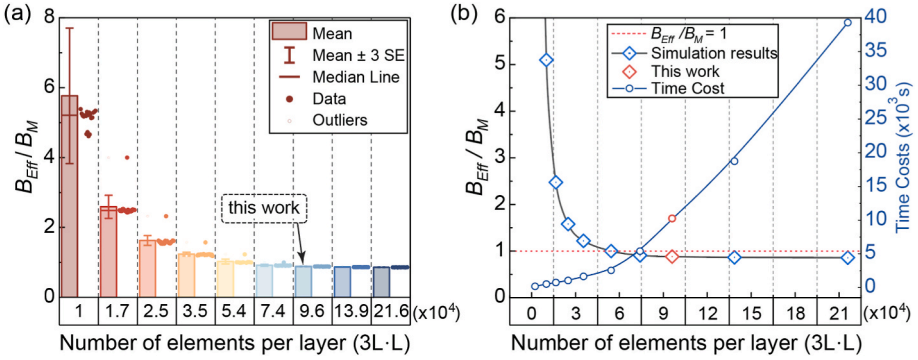

Fig. 3. Effects of the total number of elements in each layer of the higher-level $3L \times L$ rectangular structural model on the effective bending stiffness of MGPF (a) and the corresponding computational time cost (b). The basic nanoscale $L \times L$ RVE model has the number of graphene layers $M = 5$, graphene platelet area fraction $F_A = 0.987$, degree of regularity $\alpha = 0.6$, number of complete graphene platelets $N = 49$ and mean graphene platelet size $d_0 = 150$ nm.

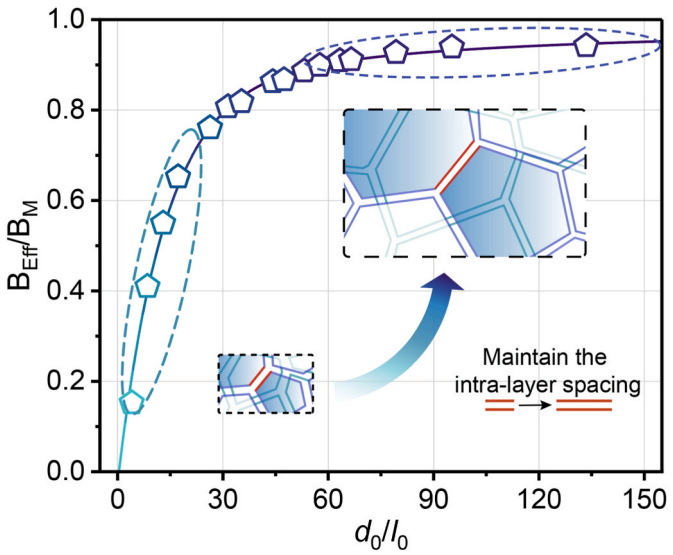

Fig. 4. Effects of the mean size of graphene platelets on the effective bending stiffness of MGPFs. The basic nanoscale $L \times L$ RVE model has 49 complete graphene platelets in each layer, number of graphene layers $M = 5$, degree of regularity $\alpha = 0.6$, and the same uniform gap of 1 nm between the intralayer neighboring graphene platelets.

and the in-plane tensile/compressive stresses in the graphene platelets are transferred *via* the out-of-plane shear deformation of the equivalent solid material for the van der Waals interaction between the staggered graphene platelets. The larger the size d_0/l_0, the larger the size of the overlap area between any two staggered graphene platelets, thus the more efficient for the stresses to be transferred inside the MGPF, and consequently the larger the bending stiffness of the MGPF, which is clearly supported by the strain contours in Figs. S2a,b,c in the Supporting Information.

According to the results in Fig. 4, the mean size of the graphene platelets can significantly affect the bending stiffness of MGPFs. In addition, the larger the mean graphene platelet size, the larger will be the total number of elements and the total degrees of freedom in the MGPF model. To minimize the possible coupled effects of the mean size of the graphene platelets, the value of d_0/l_0 should be sufficiently large. On the other hand, the computational cost should be feasible as thousands of simulations need to be performed to obtain all the data in this work. Thus, the mean graphene platelet size is fixed at $d_0/l_0 = 62.4$ (or $d_0 = 150$ nm) in the analyzes to investigate the effects of other parameters on the bending stiffness of MGPFs in the following subsections.

3.2. Effects of the area fraction of graphene platelets

For the constructed MGPF models, the graphene platelet area fraction F_A and the graphene platelet overlap ratio ρ can be obtained from the ABAQUS software according to the definitions given by Equations (1) and (2). In this subsection, all the boundary gaps between any two intralayer neighboring graphene platelets in the same MGPF model are assumed to have the same uniform width. The effects of the graphene area fraction on the effective bending stiffness of MGPFs are presented in Fig. 5a, where the bending stiffness of MGPFs has been normalized by the theoretical value B_M given by Equation (3) for the large-sized perfect multilayer graphene film. As can be seen from Fig. 5a, the normalized bending stiffness of MGPFs always increases with the increase of the graphene area fraction F_A and is approximately a quadratic function of the graphene area fraction F_A. As the individual graphene platelets in the RVE model (or MGPF) are held together by the van der Waals interaction between the staggered graphene platelets, the graphene platelet overlap ratio ρ could significantly affect the in-plane and the out-of-plane elastic properties of MGPFs [23], consequently, could also remarkably affect the bending stiffness of MGPFs.

The efficient stress transfer inside an MGPF depends on both the graphene overlap ratio ρ (i.e., F_A because $\rho = F_A^2$) and the mean graphene platelet size d_0/l_0. The mean in-plane tensile stiffness of the individual graphene platelets is approximately $T_G = D \times d_0 = 340 \times d_0$, where $D = 340$ N/m and d_0 is the mean size of the graphene platelets. The mean shear stiffness of the equivalent solid layer material for the van der Waals interaction in the overlapped area between any two staggered

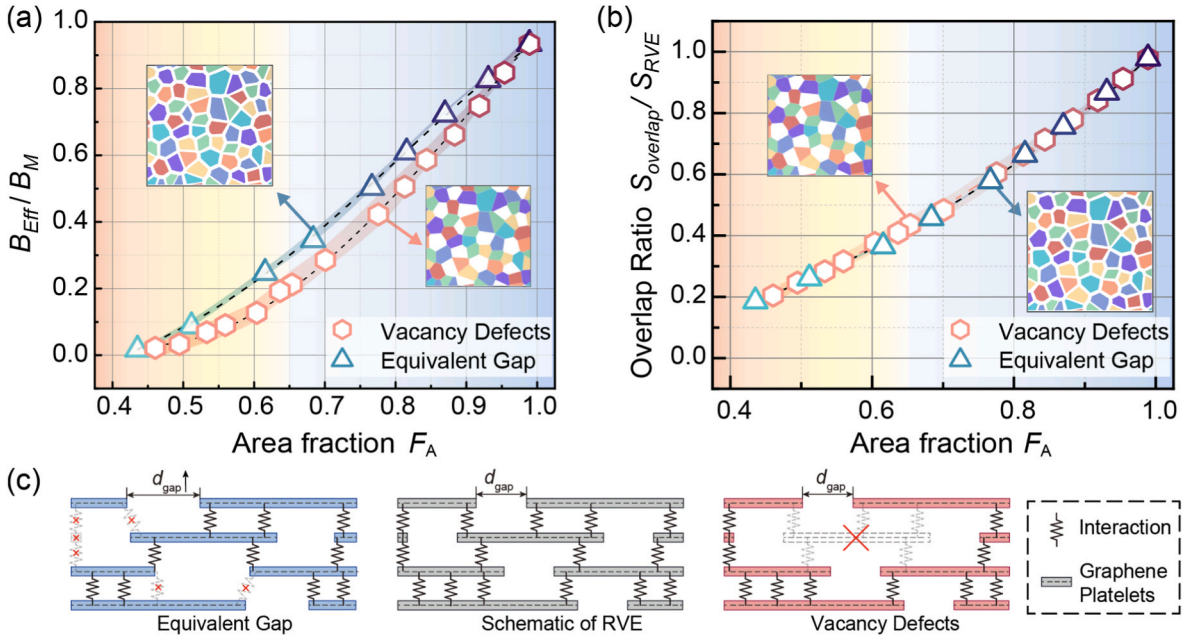

Fig. 5. (a) Effects of graphene area fraction on the normalized effective bending stiffness of MGPFs. (b) Comparison between the overlap ratios of the MGPF models with concentrated vacancy defects and with a uniform gap between any two intralayer neighboring graphene platelets. (c) Schematic of both two types of defects in the MGPF models. The basic L × *L* nanoscale RVE model has 5 graphene layers, 49 complete graphene platelets in each layer, degree of regularity $\alpha = 0.6$, and mean dimensionless graphene platelet size $d_0/l_0 = 62.4$.

graphene platelets can be approximated by $T_{vdW} = G_{vdW} \times \rho \times d_0^2/2$, where $G_{vdW} = 5$ GPa is the shear modulus of the equivalent solid layer material. If the stress transfer inside the MGPF model is mainly dependent on the shear stiffness of the overlap area, the relation $T_G > T_{vdW}$ should be satisfied, which leads to $340 > G_{vdW} \times \rho \times d_0/2 = 2.5 \times 62.4 \times 2.404 \times F_A^2 = 375 \times F_A^2$ *i.e.* $F_A < 0.952$. In other words, when $d_0/l_0 = 62.4$ and $F_A < 0.952$, the bending stiffness of MGPFs mainly depends on the shear stiffness of the overlap areas of the staggered graphene platelets. That is why the bending stiffness B_{Eff} in Fig. 5a can well be described by a quadratic function of F_A when $F_A < 0.952$. When $F_A > 0.952$, the mean tensile stiffness of the individual graphene platelets becomes smaller than the shear stiffness of the overlap area (*i.e.*, $T_G < T_{vdW}$), thus the bending stiffness B_{Eff} of MGPFs mainly depends on the tensile stiffness of MGPFs (*i.e.*, the in-plane Young's modulus E_1 of the MGPF). Obviously, the larger the graphene area fraction F_A (or the graphene overlap ratio ρ), the larger will be the bending stiffness B_{Eff} of the MGPFs, which is also confirmed by the tensile strain contours shown in Fig. S3a in the Supporting Information.

The effects of concentrated defects (or missing graphene platelets) on the bending stiffness of MGPFs are presented in Fig. 5a for comparison with those of MGPFs without missing graphene platelets. For the same value of F_A, the bending stiffnesses of MGPFs with concentrated defects (or missing graphene platelets) are always slightly smaller than those of MGPFs without missing graphene platelets, but the trends of their relations between B_{Eff} and F_A are the same. The tensile strain contours shown in Fig. S3a and S3b in Supporting Information clearly support the results in Fig. 5a. For MGPFs with either equivalent intralayer graphene platelet gaps or with concentrated defects (*i.e.*, missing graphene platelets), Fig. 5b shows that their overall graphene overlap ratios are very close if their graphene platelet area fractions are the same. Obviously, the very little difference in their overlap ratios is unlikely to cause a considerable difference between the bending stiffnesses of the two different types of MGPFs. It is noted that the relations between B_{Eff} and F_A in Fig. 5b are slightly different from those shown in Fig. 5g in literature [23] because $d_0 = 150$ nm in this work and $d_0 = 500$ nm in literature [23]. For MGPFs with a given fraction of equivalent uniform gaps between the intralayer neighboring graphene platelets, the bending stiffness (or the second moment) of the different cross-sections of the higher-level rectangular $3L \times L$ structural model along the span direction remains almost unchanged, as can be seen in Fig. 1d. In contrast, for MGPFs with the same fraction of concentrated defects (*i.e.* missing graphene platelets), the bending stiffness (or the second moment) of the different cross-sections along the span direction could vary over a much larger range. For different positive numbers a and b with $a+b = c$, there always exists the relation $2/(c/2)^2 < 1/a^n + 1/b^n$ where $n > 1$, which means that if the total amount of the defects is the same, nonuniform defects result in larger deflection or smaller stiffness. This is why the obtained bending stiffness of MGPFs with the equivalent gaps between the intralayer neighboring graphene platelets is always larger than that of MGPFs with the same fraction of concentrated defects.

3.3. Effects of the number of graphene layers

The effective bending stiffness of MGPFs strongly depends on the number M of graphene platelet layers, especially when M is smaller than 10 [33]. Fig. 6 shows the effects of M on the effective bending stiffnesses of MGPFs with a mean dimensionless graphene platelet size $d_0/l_0 = 62.4$ and different values of graphene platelet area fraction F_A, where the bending stiffnesses have been normalized by the theoretical results B_M given by Equation (3) for the perfect large-sized multilayer graphene films with the same number of graphene layers M. When $F_A = 0.987$, the normalized bending stiffness of MGPFs mainly depends on the in-plane Young's modulus of the MGPFs (as $F_A > 0.952$, see the results and discussion in the above section) and is almost a constant value of 0.925. However, if $F_A < 0.952$, *e.g.*, 0.870, 0.767 or 0.615, the normalized bending stiffnesses of MGPFs can approximately be described by the relation $B_{Eff}/B_M = F_A^2$ when the number M of the graphene platelet layers is 8 or larger. In this case, when an MGPF is bent, the load transfer efficiency mainly depends on the overlap area between the staggered graphene platelets, leading to $B_{Eff}/B_M \propto \rho \approx F_A^2$, see the explanation in above section. When $M < 8$, the normalized bending stiffness of MGPFs is smaller than but still proportional to F_A^2. The reason is because the planar-cross-section assumption to derive theoretical results in Equation (3) may not be satisfied for the bending deformation of MGPFs when $M < 8$, making the normalized bending stiffness smaller than F_A^2. More relevant results are given in Fig. S4a and b in the Supporting Information. It is noted that the regularity degree[24] of graphene platelets can also affect the bending stiffness of MGPFs, as shown in Fig. S5 and the explanation in the Supporting Information.

3.4. Comparison with relevant results obtained from 2D models

The bending stiffness of multilayer graphene films has been studied using regular or random irregular 2D models [20,34]. For the convenience to compare the normalized bending stiffness results of MGPFs obtained from the 3D random multiscale models in this work with those obtained from 2D models, three different types of 2D periodic nanoscale basic RVE models of MGPFs with the layer count $M = 5$, complete graphene platelets $N = 5$ in each layer and the same gap between any two intralayer neighboring graphene platelets are constructed as shown in Fig. 7a. The type-1 model is a fully regular model in which all the graphene platelets have the same length of d_0, and all the overlap areas

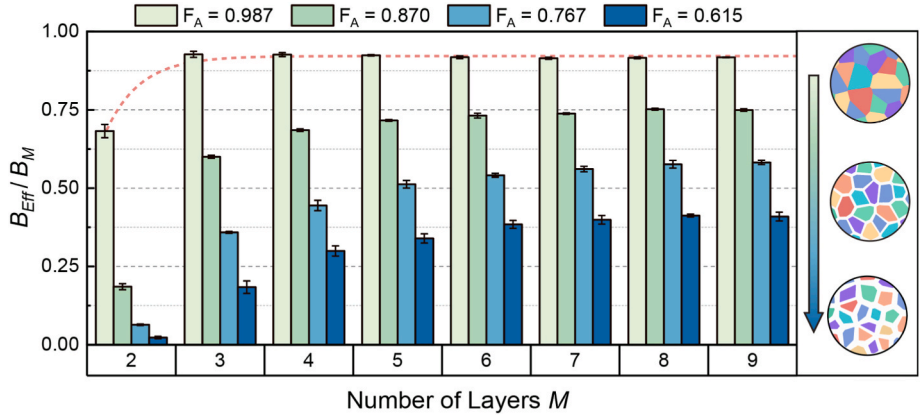

Fig. 6. Effects of the number of graphene platelet layers M on the normalized effective bending stiffnesses of MGPFs with different values of graphene platelet area fraction F_A. All the $3L \times L$ rectangular structural models of MGPFs have 3×49 complete graphene platelets in each layer, the degree of regularity $\alpha = 0.6$, and the same dimensionless mean graphene platelet size $d_0/l_0 = 62.4$.

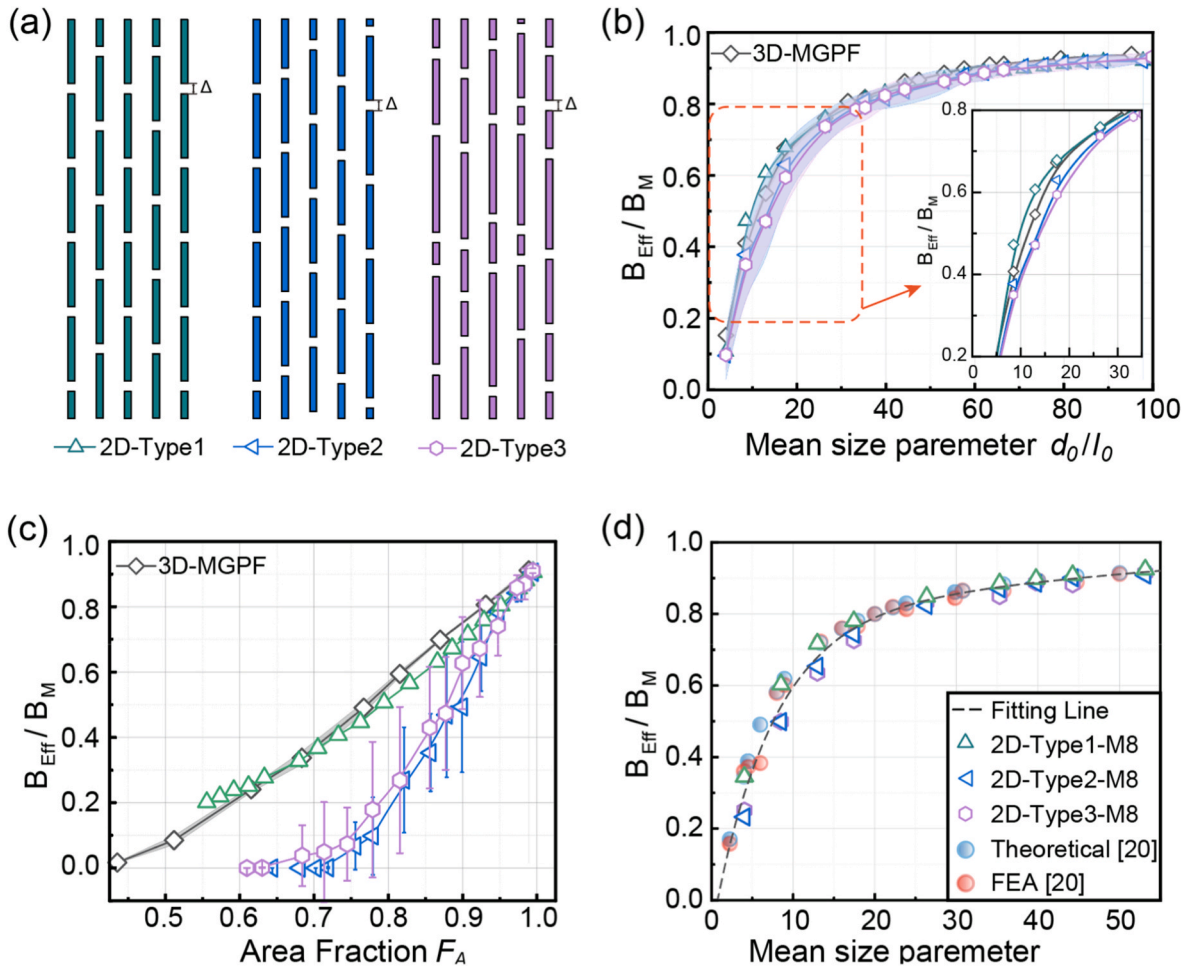

Fig. 7. (a) Schematic of the three different types of 2D periodic basic nanoscale RVE models. (b) Comparison between the curves of the normalized bending stiffness vs. the mean platelet size for 2D and 3D models, (c) Comparison of the relations between the normalized bending stiffness and the graphene area fraction F_A for 2D and 3D models (mean platelet size $d_0/l_0 = 62.4$). (d) Comparison between the trends of the normalized bending stiffness vs. the mean platelet size for the 2D models in this work and the 2D model in literature [20]. If not specified, the 3D basic nanoscale RVE model has 49 complete platelets ($N = 49$) in each layer, 5 graphene platelet layers ($M = 5$), regularity $\alpha = 0.6$; the 2D models have the parameters similar to those of the 3D models.

between any two staggered graphene platelets have the same size of approximately $d_0/2$. In the type-2 model, all the graphene platelets have the same length of d_0, and the centers of all the graphene platelets in each layer can be fully determined by a single independent random number. In the type-3 model, both the length and the centre of the individual graphene platelets are determined by independent random numbers. The dimensionless bending stiffnesses of MGPFs can be obtained from a higher-level 2D structural models composed of three identical 2D periodic basic nanoscale RVEs by FEM simulations. Similarly to the FEM treatment in the 3D models, the van der Waals interaction between the staggered graphene platelets is represented by a single layer of equivalent solid elements, and the graphene platelets are modelled as beam elements in the 2D FEM models. For more detail about the construction of the different types of 2D models, see section S6 in the Supporting Information.

The dimensionless bending stiffnesses of MGPFs obtained from the different types of 2D models are plotted against the mean graphene platelet size d_0/l_0 in Fig. 7b and against the graphene area fraction F_A in Fig. 7c, the results obtained from the 3D models are included for comparison. As can be seen in Fig. 7b, when the gap between the intralayer neighboring graphene platelets is 1 nm and the mean graphene platelet size d_0/l_0 is small, the dimensionless bending stiffnesses obtained from the random 2D models are clearly smaller than those obtained from the 3D models. The main reason is that the second moment of the cross-sections of the higher-level 3D structural model is more uniform along the span than those of the random 2D structural models, see the discussion in the above section. However, for the same mean graphene platelet size d_0/l_0, the dimensionless bending stiffness obtained from the perfect regular 2D model could be slightly larger than that obtained from the 3D model. This is because when an MGPF undergoes out-of-plane bending, the in-plane stretching/compressive load between any two intralayer neighboring graphene platelets is transferred *via* the shear deformation of the overlap areas of the van der Waals interaction between these two graphene platelets and their commonly staggered graphene platelet. Moreover, the load transfer efficiency (and thus the bending stiffness) is not only dependent on the overall graphene overlap area fraction F_A (or the overall overlap ratio ρ) – which is related to the upper limit, but more importantly limited by the smallest overlap area – which is related to the lower limit. Fig. 7c also demonstrates that when the graphene area fraction or the graphene overlap ratio is small, the dimensionless bending stiffness obtained from the perfect regular 2D model is slightly larger than that obtained from the 3D model. This is because for the same graphene overlap ratio, the perfect regular 2D model, whose lower limit is the same as the upper limit, has more efficient load transfer efficiency than the 3D model when they undergo out-of-plane bending when F_A is small. However, the bending stiffness obtained from the perfect regular 2D model is smaller than that of the 3D MGPF model when F_A is larger than 0.75. This is because all the

graphene platelet gaps in the 2D models are completely concentrated on the cross-sections of the higher-level structural model, more significantly weakening the bending stiffness of the MGPF than the 3D model. For the dimensionless bending stiffnesses obtained from the 3D models and the different types of 2D models to reach 50 %, 60 %, 70 %, 80 % and 90 % of the bending stiffness (B_M) of the perfect multilayer graphene, the required values of the mean graphene platelet size d_0/l_0 are given in Table 1 for comparison. Fig. 7d shows the comparison between the trends of the dimensionless bending stiffness vs. the mean graphene platelet size for the different types of 2D models in this work and the 2D model in literature [20], where all the models have 8 layers of graphene platelets. The results obtained from the perfect regular 2D models are slightly larger than those obtained from other models, but all the different results are quite close.

4. Versatile applications

Many natural laminated materials, *e.g.*, seashell or nacre, and artificial laminates, *e.g.*, graphene oxide films or MXene, have the same geometric characteristics as shown in Fig. 1. They all are composited of alternating hard- and soft-layers of a uniform layer thickness. Thus, the normalized (or dimensionless) bending stiffness results of MGPFs obtained in this work also apply to these different types of laminated materials. For a perfect large-sized two-phase laminated plate/film with *M* hard-layers and *M-1* soft-layers, the bending stiffness of the laminated films/plates could be approximated by the following relation

$$B_M = MB_h + \frac{D_h(t_s+t_h)^2}{12(1-\nu_h^2)}\left(M^3 - M\right) + (M-1)B_s + \frac{D_s(t_s+t_h)^2}{12(1-\nu_s^2)}\left[(M-1)^3 - (M-1)\right] \tag{4}$$

where B_h, B_s, D_h, D_s, t_h and t_s are the out-of-plane bending stiffnesses, in-plane tensile stiffnesses and layer thicknesses of the hard-phase and soft-phase monolayer materials, ν_h and ν_s are the Poisson's ratios of the hard phase and soft phase materials, respectively. It is noted that for most of the two-phase natural laminated composites such as seashell or nacre, there is no overlap between the alternating hard and soft layers in space, and both t_h and t_s are not zero. However, for large-sized perfect graphene films, the hard monolayer graphene is a single layer of atoms, its thickness t_h is so small compared to the thickness of the soft van der Waals interaction layer (which is the space between the neighboring graphene layers) and can be assumed to be zero (but $D_h = E_h \times t_h = 340$ N/m) in Equation (4). If the parameters of large-sized perfect multilayer graphene films are chosen as $D_h = 340$ N/m, $D_s = 0$, $B_h = 2.385 \times 10^{-19}$ Nm, $B_s = 0$, $t_s = 0$, and $t_h = 0.34$ nm in Equation (4), the obtained results of B_M will be the same as those given in Equation (3).

To demonstrate the versatile applications of the results obtained in this work, the bending stiffnesses of the different types of laminated materials should be normalized by those given in Equation (4), then be compared with the dimensionless results obtained in this work for MGPFs. The mean dimensionless size of the hard phase platelets of the laminated material is obtained as d_0/l_0, where $l_0 = \sqrt{D_h(t_h+t_s)/(4G_s)}$ is the shear-lag characteristic length of the laminated material. It is noted that in a typical alternating two-phase laminated material such as seashell or nacre or MGPFs, the shear modulus of the hard phase material is usually 2–3 orders larger than that of the soft phase material. Thus, the possible effect of the shear modulus of the hard phase material on the value of l_0 can be ignored. We used the same parameters to calculate the bending stiffness B_{FEA} of multi-layer plate structures using finite element software. The obtained results show that the value of B_{FEA}/B_M is between 0.95 and 0.99, increasing with the number of the layers.

In order to verify the application in MXene, graphene oxide films, for the same original 3D $L \times L$ basic nanoscale RVE models of MGPFs with $E_h = 3.7656$ TPa, $t_h = 0.987$, $d_0 = 150$ nm, $F_A = 0.987$, $M = 5$, $N = 49$, and $\alpha = 0.6$, the Young's modulus and the layer thickness of the soft layer material are alternatively varied within reasonable ranges. In this case, there are overlaps in space between the stiff shell elements and the equivalent soft layer solid elements in the FEM models, as illustrated in Fig. 8a(1). The obtained bending stiffnesses of MXene or graphene oxide films are normalized by the corresponding value of B_M and plotted against the dimensionless mean size d_0/l_0 in Fig. 8b and c, the results in Fig. 4 are also included for comparison. As can be seen, the dimensionless results between B_{Eff}/B_M and d_0/l_0 obtained from MXene or graphene oxide films with different material properties and thickness dimensions of the soft-phase material all approximately follow the same relationship obtained in Fig. 4, clearly confirming the versatile application of the obtained results in this work.

In order to validate the application in seashell or nacre-like laminated materials, for the same original 3D $L \times L$ basic nanoscale RVE models of MGPFs with $F_A = 0.987$, $M = 5$, $N = 49$, $\alpha = 0.6$, and different values of mean platelet size $d_0 = 50$, 100 or 150 nm, the Young's moduli and the layer thicknesses of soft and hard phases are systematically and alternatively varied with different ratios of E_h/E_s (400, 200, 100, 40, 20) and t_h/t_s (0.2, 0.5, 1, 2, 5). In this case, both the hard and soft phases are represented by single- or multi-layer solid elements depending on their relative layer thickness and there is no overlap in space between the stiff phase solid elements and the soft phase solid elements in the FEM models, as illustrated in Fig. 8a(2). The obtained bending stiffnesses of the seashells or nacre-like materials are normalized by the corresponding values of B_M given by Equation (4) and plotted against the dimensionless mean size d_0/l_0 in Fig. 8d, with the results in Fig. 4 included for comparison. As can be seen, the dimensionless results between B_{Eff}/B_M and d_0/l_0 obtained from seashell or nacre-like laminated materials with different mean platelet sizes, different material properties and thickness dimensions of the soft and stiff component materials all well follow the same relationship obtained in Fig. 4, well vindicating the versatile application of the obtained results in this work.

Table 1
The mean dimensionless size d_0/l_0 of graphene platelets required for the bending stiffness B_{Eff} obtained from the 3D model of MGPFs, and the three types of 2D models to reach 50 %, 60 %, 70 %, 80 %, 90 % of the bending stiffness (B_M) of the perfect large-sized multilayer graphene films. All the higher-level $3L \times L$ rectangular structural models of MGPFs have 3×49 complete graphene platelets in each layer, the degree of regularity $\alpha = 0.6$, and the same intra-layer gap 1 nm between any intralayer neighboring graphene platelets.

Model	50 %	60 %	70 %	80 %	90 %
2D Type-1	10.0	13.1	20.0	35.2	72.3
2D Type-2	13.6	16.8	23.3	35.3	72.6
2D Type-3	14.0	17.4	24.5	35.3	72.5
Our 3D random model	11.35	15.0	20.5	28.9	49.8

5. Conclusion

As it is very difficult to produce large-sized perfect graphene films, it is necessary to assemble graphene or graphene-oxide platelets into macroscale multilayer structures, such as graphene assemblies and MXene membranous materials. While numerous experimental studies have demonstrated that a reduction in mechanical properties is inevitable during this process, there remains a significant potential to enhance the properties and reliability. By optimizing the geometric configuration of multilayer macroscopic assemblies, such as graphene films, graphene paper, and MXene composite films, the mechanical properties of these materials can be brought closer to their ideal results. This is particularly important given the substantial disparity in the mechanical properties between large-sized perfect multilayer films and their macroscopic multilayer platelet counterparts.

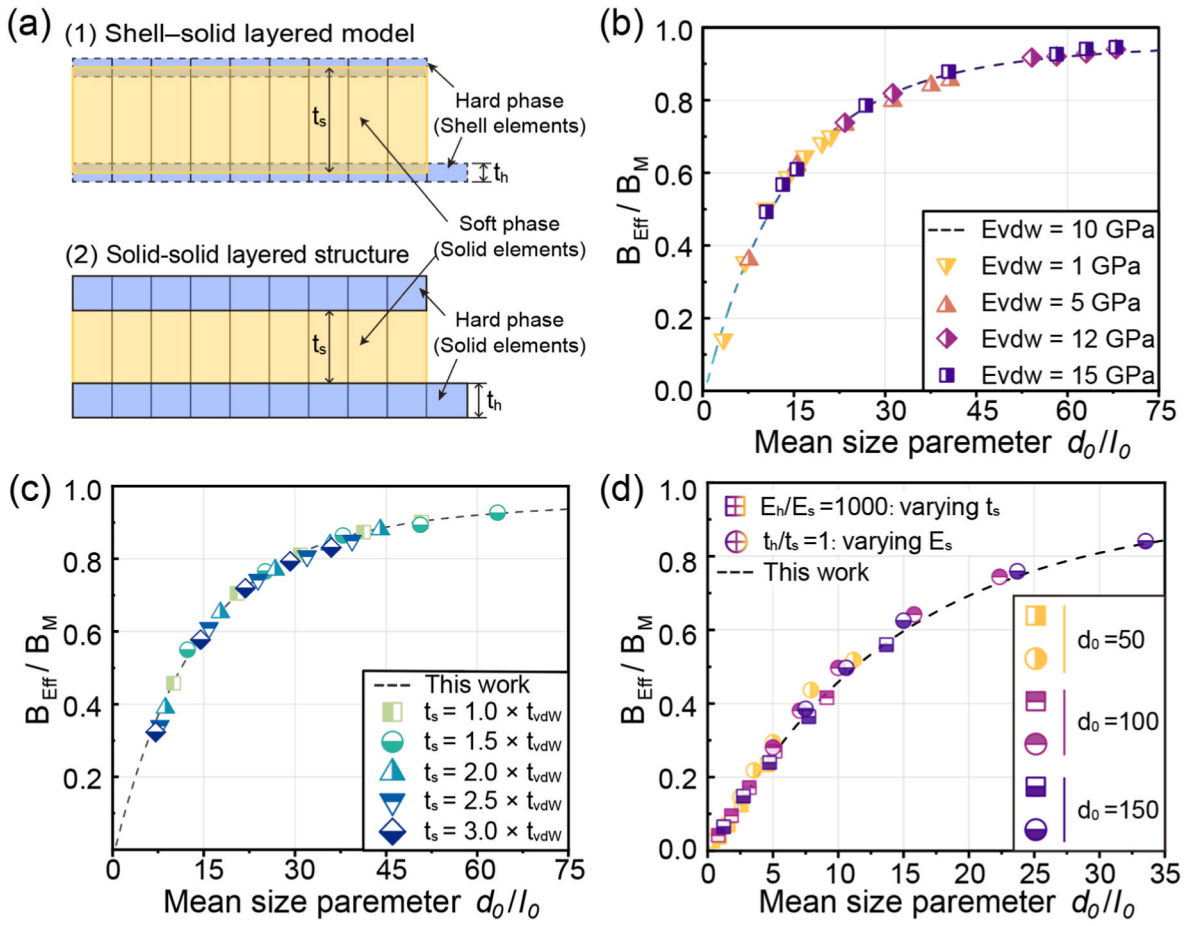

Fig. 8. (a) Schematic of the shell–solid layered model (MGPFs used in this work) and the solid–solid layered model. (b, c) Normalized bending stiffness vs. dimensionless size (d_0/l_0) for the shell-solid layered model, (b) effect of Young's modulus variation; (c) effect of interlayer thickness variation. (d) Normalized bending stiffness vs. dimensionless size d_0/l_0 for both structural models under varying interlayer parameters. All the $3L \times L$ higher-level rectangular models of MGPFs have 3×49 complete graphene platelets in each layer, the degree of regularity $\alpha = 0.6$, and the same mean size $d_0/l_0 = 62.4$.

This study systematically analyzes the bending stiffness of nacre-like MGPFs through thousand finite element simulations using realistic multiscale 3D models, quantifying the effects of geometric parameters, such as mean graphene platelet size, graphene area fraction and number of graphene platelet layers, on the effective bending stiffness of MGPFs. It is further demonstrated that the normalized results apply to different types of multilayer materials such as MXene and graphene oxide (GO) films, nacre and seashells. It is worth noting that the research in this work is fully focused on small curvature bending stiffness. At the moment, we are actually working on the large curvature bending behavior of MGPFs in which the bending deformation involves delamination, and the bending stiffness is a nonlinear function of the bending curvature when the curvature is very large. The results in this work help pave the way to achieve reliable and maximum possible bending stiffness of these different types of multi-layered materials.

CRediT authorship contribution statement

Penghao Qi: Writing – review & editing, Writing – original draft, Visualization, Validation, Methodology, Investigation, Formal analysis, Data curation. **Xindong Chen:** Investigation, Formal analysis. **Hanxing Zhu:** Writing – review & editing, Writing – original draft, Validation, Supervision, Methodology, Investigation, Formal analysis, Conceptualization. **Yongtao Lyu:** Investigation, Formal analysis. **Qing Peng:** Investigation, Formal analysis.

Data Availability statement

The data and findings of this study are available from the corresponding authors on reasonable request.

Declaration of competing interest

The authors do not have conflict interest.

Acknowledgements

Penghao Qi would like to thank the support of China Scholarship Council (No. 202106280043) for sponsoring his PhD study at Cardiff University.

Appendix A. Supplementary data

Supplementary data to this article can be found online at https://doi.org/10.1016/j.carbon.2025.121023.

References

[1] S. Wan, X. Li, Y. Chen, N. Liu, Y. Du, S. Dou, L. Jiang, Q. Cheng, High-strength scalable MXene films through bridging-induced densification, Science 374 (2021) 96–99, https://doi.org/10.1126/science.abg2026.
[2] Y. Zhang, S. Gong, Q. Zhang, P. Ming, S. Wan, J. Peng, L. Jiang, Q. Cheng, Graphene-based artificial nacre nanocomposites, Chem. Soc. Rev. 45 (2016) 2378–2395, https://doi.org/10.1039/C5CS00258C.

[3] W. Yu, K. Gong, Y. Li, B. Ding, L. Li, Y. Xu, R. Wang, L. Li, G. Zhang, S. Lin, Flexible 2D materials beyond graphene: synthesis, properties, and applications, Small 18 (2022) 2105383, https://doi.org/10.1002/smll.202105383.
[4] M.Y. Khalid, R. Umer, Y.H. Zweiri, J.-K. Kim, Rise of graphene in novel piezoresistive sensing applications: a review on recent development and prospect, Mater. Sci. Eng. R Rep. 163 (2025) 100891, https://doi.org/10.1016/j.mser.2024.100891.
[5] C. Hou, S. Zhang, R. Liu, T. Gemming, A. Bachmatiuk, H. Zhao, H. Jia, S. Huang, W. Zhou, J.-B. Xu, J. Pang, M.H. Rümmeli, J. Bi, H. Liu, G. Cuniberti, Boosting flexible electronics with integration of two-dimensional materials, InfoMat 6 (2024) e12555, https://doi.org/10.1002/inf2.12555.
[6] Y. Li, W. Lian, Q. Cheng, High-performance nacre-inspired 2D carbon-based nanocomposites, Adv. Mater. n/a (2025) 2501932, https://doi.org/10.1002/adma.202501932.
[7] S. Wan, Y. Chen, Y. Wang, G. Li, G. Wang, L. Liu, J. Zhang, Y. Liu, Z. Xu, A. P. Tomsia, L. Jiang, Q. Cheng, Ultrastrong graphene films via long-chain π-Bridging, Matter 1 (2019) 389–401, https://doi.org/10.1016/j.matt.2019.04.006.
[8] T. Zhou, H. Ni, Y. Wang, C. Wu, H. Zhang, J. Zhang, A.P. Tomsia, L. Jiang, Q. Cheng, Ultratough graphene–black phosphorus films, Proc. Natl. Acad. Sci. 117 (2020) 8727–8735, https://doi.org/10.1073/pnas.1916610117.
[9] S. Wan, L. Jiang, Q. Cheng, Design principles of high-performance graphene films: interfaces and alignment, Matter 3 (2020) 696–707, https://doi.org/10.1016/j.matt.2020.06.023.
[10] D. Lai, Z. Chen, Z. Han, Z.-S. Wu, X. Chen, Progress and roadmap for graphene films in electromagnetic interference shielding, Resour. Chem. Mater. 2 (2023) 11–38, https://doi.org/10.1016/j.recm.2022.12.001.
[11] H. Zheng, P. He, S. Yang, Y. Lu, N. Guo, Y. Li, G. Wang, G. Ding, Achieving ultra-high heat flux transfer in graphene films via tunable gas escape channels, Adv. Sci. 12 (2025) 2410913, https://doi.org/10.1002/advs.202410913.
[12] H.B. Park, J. Kamcev, L.M. Robeson, M. Elimelech, B.D. Freeman, Maximizing the right stuff: the trade-off between membrane permeability and selectivity, Science 356 (2017) eaab0530, https://doi.org/10.1126/science.aab0530.
[13] H. Ren, L. Zheng, G. Wang, X. Gao, Z. Tan, J. Shan, L. Cui, K. Li, M. Jian, L. Zhu, Y. Zhang, H. Peng, D. Wei, Z. Liu, Transfer-medium-free nanofiber-reinforced graphene film and applications in wearable transparent pressure sensors, ACS Nano 13 (2019) 5541–5548, https://doi.org/10.1021/acsnano.9b00395.
[14] Y. Yan, X.-Q. Feng, Synergistic toughening mechanisms of macro- and micro-structures in nacre: effects of T-stresses, J. Mech. Phys. Solid. 197 (2025) 106067, https://doi.org/10.1016/j.jmps.2025.106067.
[15] F. Barthelat, Designing nacre-like materials for simultaneous stiffness, strength and toughness: optimum materials, composition, microstructure and size, J. Mech. Phys. Solid. 73 (2014) 22–37, https://doi.org/10.1016/j.jmps.2014.08.008.
[16] E. Han, J. Yu, E. Annevelink, J. Son, D.A. Kang, K. Watanabe, T. Taniguchi, E. Ertekin, P.Y. Huang, A.M. van der Zande, Ultrasoft slip-mediated bending in few-layer graphene, Nat. Mater. 19 (2020) 305–309, https://doi.org/10.1038/s41563-019-0529-7.
[17] M. Trushin, A.H. Castro Neto, Stability of a Rolled-Up conformation state for two-dimensional materials in aqueous solutions, Phys. Rev. Lett. 127 (2021) 156101, https://doi.org/10.1103/PhysRevLett.127.156101.
[18] I. Nikiforov, D.-M. Tang, X. Wei, T. Dumitrică, D. Golberg, Nanoscale bending of multilayered boron nitride and graphene ribbons: experiment and objective molecular dynamics calculations, Phys. Rev. Lett. 109 (2012) 025504, https://doi.org/10.1103/PhysRevLett.109.025504.
[19] G. Wang, Z. Dai, J. Xiao, S. Feng, C. Weng, L. Liu, Z. Xu, R. Huang, Z. Zhang, Bending of Multilayer van der Waals Materials, Phys. Rev. Lett. 123 (2019) 116101, https://doi.org/10.1103/PhysRevLett.123.116101.
[20] Y. Chen, H. Liu, K. Pang, C. Zhang, H. Qin, Z. Xu, Y. Liu, Bending deformable tension-shear model for nacre-like composites, J. Mech. Phys. Solid. 171 (2023) 105132, https://doi.org/10.1016/j.jmps.2022.105132.
[21] H. Qin, Y. Yan, H. Liu, J. Liu, Y.-W. Zhang, Y. Liu, Modified Timoshenko beam model for bending behaviors of layered materials and structures, Extreme Mech. Lett. 39 (2020) 100799, https://doi.org/10.1016/j.eml.2020.100799.
[22] Z. Huang, Z. He, Y. Zhu, H. Wu, A general theory for the bending of multilayer van der Waals materials, J. Mech. Phys. Solid. 171 (2023) 105144, https://doi.org/10.1016/j.jmps.2022.105144.
[23] P. Qi, X. Chen, H. Zhu, Y. Lyu, B. Zhang, Q. Peng, X. Feng, T. Fan, D. Zhang, Quantifying the effects of geometric parameters on the elastic properties of multilayer graphene platelet films, Adv. Mater. n/a (2025) 2502546, https://doi.org/10.1002/adma.202502546.
[24] H.X. Zhu, J.R. Hobdell, A.H. Windle, Effects of cell irregularity on the elastic properties of 2D Voronoi honeycombs, J. Mech. Phys. Solid. 49 (2001) 857–870, https://doi.org/10.1016/S0022-5096(00)00046-6.
[25] A. Hardy, J. Dix, C.D. Williams, F.R. Siperstein, P. Carbone, H. Bock, Design rules for graphene and carbon nanotube solvents and dispersants, ACS Nano 12 (2018) 1043–1049, https://doi.org/10.1021/acsnano.7b05159.
[26] P.H. Tan, W.P. Han, W.J. Zhao, Z.H. Wu, K. Chang, H. Wang, Y.F. Wang, N. Bonini, N. Marzari, N. Pugno, G. Savini, A. Lombardo, A.C. Ferrari, The shear mode of multilayer graphene, Nat. Mater. 11 (2012) 294–300, https://doi.org/10.1038/nmat3245.
[27] Y. Wang, S. Feng, D. Peng, T. Li, C. Zheng, Z. Cai, Z. Wu, Q. Zheng, Z. Xu, Intrinsic interlayer shear strength of graphite, J. Mech. Phys. Solid. 193 (2024) 105853, https://doi.org/10.1016/j.jmps.2024.105853.
[28] P. Koskinen, O.O. Kit, Approximate modeling of spherical membranes, Phys. Rev. B 82 (2010) 235420, https://doi.org/10.1103/PhysRevB.82.235420.
[29] K.S. Novoselov, A.K. Geim, S.V. Morozov, D. Jiang, Y. Zhang, S.V. Dubonos, I. V. Grigorieva, A.A. Firsov, Electric field effect in atomically thin carbon films, Science 306 (2004) 666–669, https://doi.org/10.1126/science.1102896.
[30] Q. Peng, C. Liang, W. Ji, S. De, A theoretical analysis of the effect of the hydrogenation of graphene to graphane on its mechanical properties, Phys. Chem. Chem. Phys. 15 (2013) 2003–2011, https://doi.org/10.1039/C2CP43360E.
[31] Y. Liu, B. Xie, Z. Zhang, Q. Zheng, Z. Xu, Mechanical properties of graphene papers, J. Mech. Phys. Solid. 60 (2012) 591–605, https://doi.org/10.1016/j.jmps.2012.01.002.
[32] H. Gao, B. Ji, I.L. Jäger, E. Arzt, P. Fratzl, Materials become insensitive to flaws at nanoscale: lessons from nature, Proc. Natl. Acad. Sci. 100 (2003) 5597–5600, https://doi.org/10.1073/pnas.0631609100.
[33] D.G. Papageorgiou, I.A. Kinloch, R.J. Young, Mechanical properties of graphene and graphene-based nanocomposites, Prog. Mater. Sci. 90 (2017) 75–127, https://doi.org/10.1016/j.pmatsci.2017.07.004.
[34] Y. Yan, Z.-L. Zhao, X.-Q. Feng, H. Gao, Nacre's brick–mortar structure suppresses the adverse effect of microstructural randomness, J. Mech. Phys. Solid. 159 (2022) 104769, https://doi.org/10.1016/j.jmps.2021.104769.